

Comparison of numerical and analytical solutions for fly casting dynamics

Caroline Gatti-Bono* and N. C. Perkins†

*Applied Numerical Algorithms, NERSC, Lawrence Berkeley National Laboratory, Berkeley, CA 94720, USA

†Department of Mechanical Engineering, University of Michigan, Ann Arbor, MI 48109, USA

Abstract

This paper presents an approximate analytical model of the dynamics of a tapered fly line during a standard overhead cast. During casting, the line forms a nonlinear propagating wave that is frequently referred to as a 'loop' by fly casters. The geometry of the loop is prescribed by three distinct parts: a straight bottom segment (attached to a stationary fly rod), a semi-circular segment that is propagating (i.e. the loop), and a straight top segment that is also propagating, (i.e. the traveling line). A fly (particle) is attached at the end of the traveling line. A work–energy balance yields the velocity of the fly as a function of the length of the traveling line. For a uniform fly line (level line), a closed-form solution is found, while for a tapered fly line, the solution is obtained by quadrature. A critical loop diameter arises in the analysis, and it determines whether the final velocity of the fly is greater or lesser than the initial velocity of the traveling line. The analytical solutions are critically compared against numerical solutions of a general model for fly line dynamics that relaxes many of the assumptions employed in the analytical model. The agreement between the two solutions remains close during the loop propagation phase, provided a significant amount of fly line remains in the traveling line. However, as the traveling line vanishes and the loop 'turns over', the two solutions diverge abruptly due to the many simplifying assumptions employed in the analytical model.

Keywords: Fly casting dynamics; Numerical model; Analytical approximation; Elastica.

Introduction

A significant challenge in the sport of fly fishing is to cast an artificial 'fly' to a feeding fish. To this end, a fly fisher utilizes a fly rod to cast a weighted fly line that terminates with a short 'leader', and then the fly. The most commonly used casting style is the standard overhead cast as illustrated in Figure 1. The sketches

therein illustrate four main stages of the forward cast portion of an overhead cast. The first stage starts with the fly line laid out horizontally behind the caster at the conclusion of a *back cast*; see Figure 1(a). The caster then rotates the fly rod clockwise, accelerates the fly line, and then abruptly stops the rod as illustrated in Figure 1(b). From this point onwards, the end of the fly line attached to the rod tip remains stationary and a *loop* necessarily forms between the moving (upper) portion of the fly line and the stationary (lower) portion of the fly line; see Figure 1(b). From the perspective of dynamics, this loop represents a nonlinear wave that propagates forward as shown in Figure 1(c) until it reaches the end of the fly line

Correspondence address:

Prof. Noel Perkins
Mechanical Engineering, University of Michigan
2250 G. G. Brown
Ann Arbor, MI, 48109-2125, USA
e-mail: ncp@umich.edu

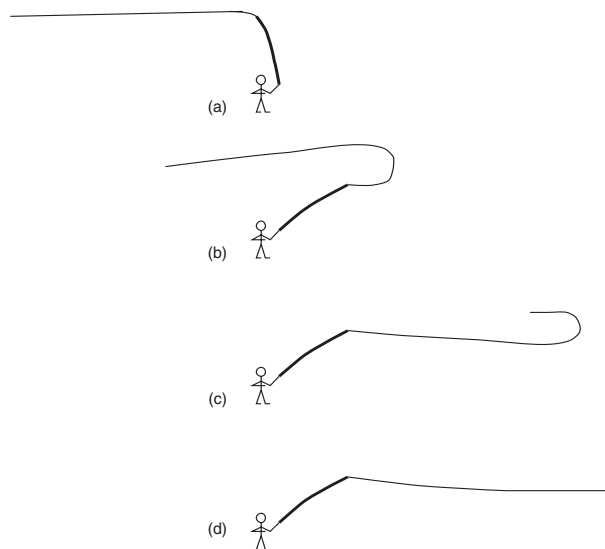


Figure 1 The forward cast of an overhead cast. (a) Perfectly laid out back cast; (b) just after stop of forward cast; (c) loop propagation; (d) completion of cast (loop turnover).

where the loop *turns over*. This final turnover occurs on or near the surface of the water and the cast is complete.

Realizing such a cast often requires considerable practice and instruction. Fly casting instructors emphasize the importance of understanding the mechanics of the fly rod and fly line as the basis for improved casting. Our overall understanding of fly casting mechanics can be sharpened by studying mathematical models of loop dynamics. Several previous studies that have contributed models for loop dynamics are here reviewed.

Spolek (1986) uses the work–energy principle to model loop propagation after the loop has fully formed. The line is composed of three segments: a straight bottom segment that is attached to a stationary rod, a semi-circular segment that is propagating (i.e. the loop), and a straight top segment that is also propagating, referred to as the ‘traveling line’. A fly is attached at the end of the traveling line. Spolek considers the kinetic energies of the traveling line and of the fly (but ignores the kinetic energy of the loop), and the energy dissipated by drag forces acting on the entire fly line (traveling line and loop) and on the fly. To estimate drag, the loop is modelled as a cylinder in cross-flow. Both level lines and tapered lines are considered; however, the taper is modelled as an abrupt

change in line diameter instead of a smooth change. Application of overall work/energy balance leads to a numerical solution for the velocity of the fly as a function of the fly position and the conclusion that tapered lines and level lines behave qualitatively differently. Lingard (1988) proposes an improvement to Spolek’s drag model and notes that the use of Morison’s equations for the drag results in a 30% reduction of the work done by drag on the loop. In the first part of his study, Robson (1990) deduces an analytical solution to a model similar to Spolek’s (1986) by replacing the semi-circular segment (the loop) by a straight vertical segment of line (i.e. a rectangular loop). The kinetic energy of the loop is included, however, the energy dissipated by drag forces on the traveling line and the fly are ignored as is any taper of the fly line. He provides a closed-form solution for the fly velocity as a function of the fly displacement for a level line and introduces a ‘critical loop diameter’. For loops smaller than the critical loop, the velocity of the fly will increase during the cast. Otherwise, the velocity of the fly will decrease.

It is important to emphasize that in all the analytical models above, the loop is highly idealized. It is either considered to be a perfect semi-circle or a rectangle of prescribed dimensions. Moreover, the line is either level or crudely tapered and drag is modelled partially or not completely on all segments. These restrictions together with the fact that the remainder of the cast is unmodelled, significantly restrict the utility of these approximations to model actual fly casting.

A more complete model of an overhead cast is developed by Gatti & Perkins (2001) and Gatti-Bono & Perkins (2002) who utilize a continuum model for a smoothly tapered fly line. The fly line is modelled as a long elastica that is allowed to undergo arbitrarily large rotations. The model accounts for fly line tension (or compression), bending, aerodynamic drag, and weight, and the formulation allows one to work directly with the physical parameters of the fly line, including density and taper information. A numerical algorithm is presented to solve the resulting initial two-point, boundary-value problem, and sample problems are analyzed that highlight the fundamental features of fly casting dynamics. This model, however, requires that the motion (path) of the rod tip be pre-

scribed, and it does not account for the coupled dynamics of the fly rod. A later study (Gatti, 2002) presents a numerical model for the dynamics of the fully coupled fly line/ fly rod system and companion experimental results. The study by Hendry & Hubbard (2000) includes a refined finite element model of a fly rod and the attached fly line as modelled using truss elements. Key features of the rod dynamics including the motion of the rod tip are discussed.

In this paper, we will compare the idealized analytical solutions based on work–energy during loop propagation, with numerical simulations obtained in the study by Gatti-Bono & Perkins (2002). In doing so we will also generalize the analytical solutions to describe a line with smooth (realistic) taper and drag on all moving segments. We begin by reviewing the existing analytical approximations and identify the extensions considered herein. Solutions for the extended model are derived and then critically compared to the results of the (general) numerical model.

Analytical model

After a brief review of previous analytical models, we develop a new closed-form solution for a level line, and a new analytical solution via quadrature for a tapered line.

Brief review of previous analytical models

Level lines, although seldom used in practice, are a good first approximation to tapered lines and lead to a significant simplification of the analytical model. Solutions for the fly velocity as a function of the fly displacement are available for level lines; see Lingard (1988), Robson (1990), and Spolek (1986). These solutions however omit terms in either the computation of the kinetic energy or the work done by drag. Spolek (1986) and Lingard (1988) omit the kinetic energy of the loop but they do account for the work done by drag. They both arrive at their final solution by numerical analysis. Robson (1990) omits the work done by drag on the fly and the traveling line but does include the kinetic energy of the loop. He arrives at a closed-form solution. The analytical approximations developed in this section include the kinetic energies of the fly, the traveling line, and the loop, and the

energy dissipated by drag acting on the fly, the traveling line, and the loop. Moreover, we arrive at a closed-form solution for the case of a level line and at a simple integral solution for the case of a (realistically) tapered line.

Level fly line

The model of an overhead cast is depicted in Figure 2. The fly line is divided into three segments: a bottom straight segment that is attached to a stationary rod tip, a semi-circular segment of radius R ('the loop') that is propagating to the left, and an upper straight segment of length $l(t)$, referred to as the traveling line, that is propagating to the left with velocity $v(t)$. A fly of radius r_f , mass m_f and drag coefficient C_f is attached to the end of the traveling line.

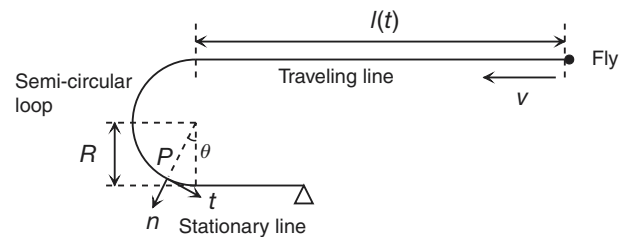


Figure 2 Simplified model of an overhead cast.

The work–energy balance for the fly and fly line systems can be written

$$\frac{1}{2} m_{tl}(t)v^2(t) + \frac{1}{2} m_f v^2(t) + T_l(t) = T_0 - \int_0^t \delta \dot{W}_{dt}(u) du - \int_0^t \delta \dot{W}_l(u) du - \int_0^t \delta \dot{W}_f(u) du \tag{1}$$

Here, $v(t)$ is the velocity of the traveling line and the attached fly;

$$m_{tl}(t) = \rho_l \frac{\pi d_l^2}{4} l(t)$$

is the mass of the traveling line; ρ_l is the density of the fly line; d_l is the diameter of the fly line; m_f is the mass of the fly; $T_l(t)$ is the kinetic energy of the loop; T_0 is the initial kinetic energy of the fly and fly line system; $\delta \dot{W}_{dt}(t)$ is the power dissipated by the drag acting on the traveling line; $\delta \dot{W}_l(t)$ is the power dissipated by the drag acting on the loop; $\delta \dot{W}_f(t)$ is the power dissipated by the drag acting on the fly.

The velocity components of a point P on the loop is given by

$$v_t(t) = \frac{v(t)}{2}(1 - \cos(\theta)) \tag{2}$$

$$v_n(t) = \frac{v(t)}{2}\sin(\theta) \tag{3}$$

Where $v_t(t)$ is the velocity component in the tangential direction, $v_n(t)$ is the velocity component in the normal direction, and θ is the angle defined in Figure 2. Equations (2)–(3) are used to compute the quantities $T(t)$, $\delta\dot{W}_t(t)$, $\delta\dot{W}_n(t)$ and $\delta\dot{W}_f(t)$, as given in Appendix A.

Using the results of Appendix A, equation (1) can be rewritten as:

$$\frac{1}{2}M(l(t))v^2(t) = T_0 - \int_0^t \Gamma(l(u))v^3(u)du \tag{4}$$

where

$$M(l(t)) = \rho_l \frac{\pi d_l^2}{4} l(t) + \frac{\rho_l \pi^2 d_l^2 R}{8} + m_f = \alpha(l(t) + \beta)$$

$$\Gamma(l(t)) = \frac{1}{2} \rho_a C_t d_t \pi l(t) + \rho_a d_t R \left(\frac{5\pi^2}{32} C_t + \frac{1}{12} C_n \right) + \frac{1}{2} \rho_a C_f \pi r_f^2 \tag{6}$$

$$= \frac{\lambda \alpha}{2} (l(t) + \mu) \tag{7}$$

Here, ρ_a is the density of air; C_t is the tangential drag coefficient of the fly line; C_n is the normal drag coefficient of the fly line; C_f is the drag coefficient of the fly; r_f is the effective radius of the fly. Defining the four constants

$$\alpha = \rho_l \frac{\pi d_l^2}{4} \tag{8}$$

$$\beta = \frac{\pi R}{2} + \frac{4m_f}{\rho_l \pi d_l^2} \tag{9}$$

$$\lambda = \frac{4\rho_a C_t}{\rho_l d_l} \tag{10}$$

$$\mu = 2 \frac{d_t R \left(\frac{5\pi^2}{32} + \frac{1}{12} C_n \right) + \frac{1}{2} C_f \pi r_f^2}{C_t d_t \pi} \tag{11}$$

allows one to simplify (5)–(6) as shown. These results will now be used to compute the velocity of the fly as the cast develops. Note from Figure 3 that the distance $x(t)$ traveled by the fly is

$$x(t) = l_0 - y(t) = l_0 - (2l(t) - l_0) = 2(l_0 - l(t)) \tag{12}$$

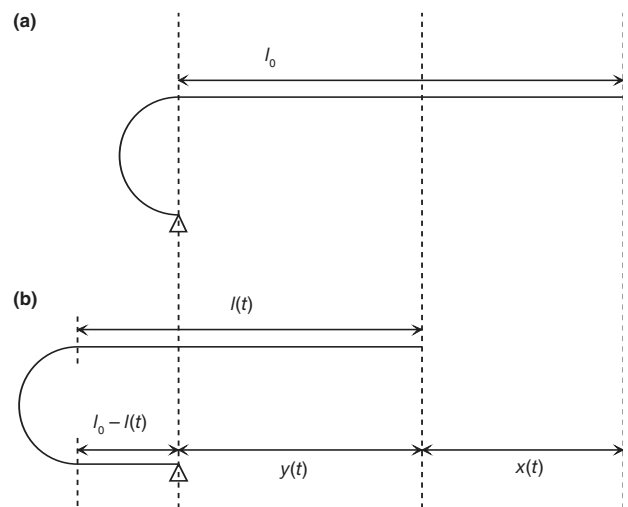


Figure 3 Configuration of the fly line (a) at time $t = 0$ s, and (b) at time t .

Differentiating equation (4) with respect to time, dividing by $v(t)$ (the loop is propagating so $v(t) \neq 0$) and using the fact that $v(t) = \dot{x}(t) = -2\dot{l}(t)$, yields a nonlinear differential equation in $l(t)$

$$M(l(t))\dot{l}(t) = \left(2\Gamma(l(t)) - \frac{1}{2}M'(l(t)) \right) \dot{l}^2(t) \tag{13}$$

Equation (13) can be integrated (see Appendix B for details), and yields the velocity of the fly as a function of the length of the traveling line

$$v(l(t)) = v_0 e^{\lambda(l(t) - l_0)} \left(\frac{l_0 - \beta}{l(t) + \beta} \right)^{1/2 + \lambda(\beta - \mu)} \tag{14}$$

Equation (14) differs from that found by Robson (1990) mainly due to the (decreasing) exponential factor. This factor arises here due to the inclusion of

skin friction (C_f) that was neglected by Robson (1990). The exponential factor (drag) also assures that the velocity of the loop or fly will eventually decrease as the cast is continually lengthened (l_0 increases) when all other parameters are held constant. Thus, a fly fisher will try to maintain loop speed by developing a higher line speed v_0 (rod tip speed) to initially launch the loop for longer casts. This entire effect is lost if the model does not include drag.

We now study the limiting case of a level line without air drag. Conservation of energy now holds and the constant kinetic energy becomes focused to a decreasing portion of moving fly line. The fly therefore accelerates as the cast evolves as confirmed by the result:

$$v(l(t)) = v_0 \sqrt{\left(\frac{l_0 - \beta}{l(t) + \beta}\right)} \quad (15)$$

which follows from (14) upon eliminating the influence of drag ($\lambda = \mu = 0$). If, in addition, we now eliminate the kinetic energy of the loop and fly, then $\beta = 0$ and in this case, the result above shows that the fly line velocity becomes unbounded at the end of the cast ($l(t) \rightarrow 0$). Thus, this non-physical limit is avoided by the inclusion of loop and fly kinetic energy.

Equation (14) also provides a means to analyze fundamental characteristics of the fly cast with drag,

including the conditions needed for the fly to accelerate or decelerate as the cast evolves. To this end, compute the derivative of equation (14) with respect to $l(t)$

$$v'(l(t)) = v_0 \exp(\lambda(l(t) - l_0)) \left(\frac{l_0 - \beta}{l(t) + \beta}\right)^{1/2 + \lambda(\beta - \mu)} \left(\lambda - \left(\frac{1}{2} + \lambda(\beta - \mu)\right) \frac{1}{l(t) + \beta}\right) \quad (16)$$

and introduce two characteristic diameters D_{min} and D_{max} , as follows

$$D_{min} = 2 \frac{\frac{\pi}{16} \rho_l d_l^2 - \frac{1}{2} \rho_a C_f \pi r_f^2 - \frac{1}{2} \rho_a C_t d_l \pi l_0}{\rho_a d_l \left(\frac{5\pi^2}{32} C_t + \frac{1}{12} C_n\right)} \quad (17)$$

$$D_{max} = 2 \frac{\frac{\pi}{16} \rho_l d_l^2 - \frac{1}{2} \rho_a C_f \pi r_f^2}{\rho_a d_l \left(\frac{5\pi^2}{32} C_t + \frac{1}{12} C_n\right)} \quad (18)$$

We now analyze three cases that distinguish whether the fly will accelerate or decelerate during the cast (for a level line). Examples of these cases are given in Figure 4.

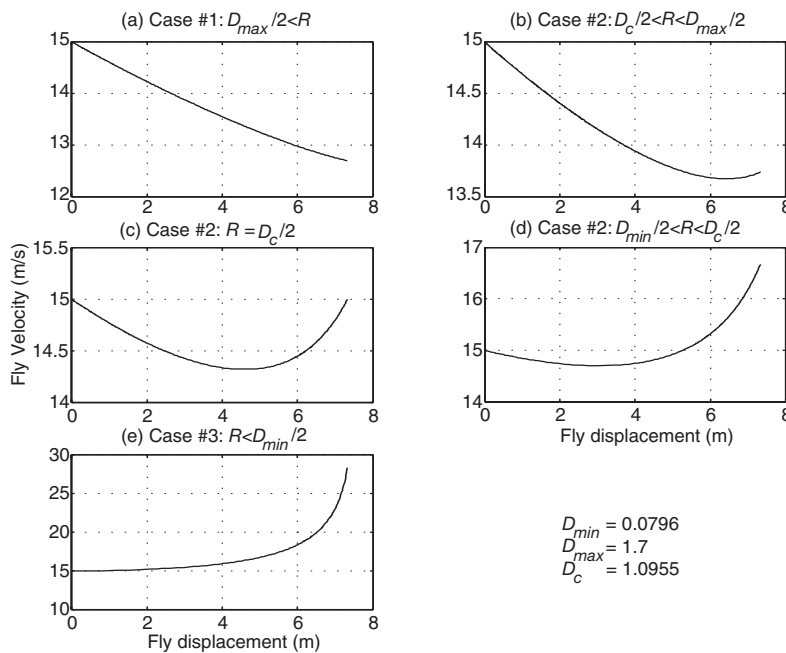


Figure 4 Approximate analytical solutions for a level line for different loop diameters. Remaining casting parameters are defined in Table 1. (a) $D = 2$ m, (b) $D = 1.5$ m, (c) $D = 1.0955$ m, (d) $D = 0.75$ m, and (e) $D = 0.05$ m.

Table 1 Parameters that characterize a level line equivalent to the tapered line presented in this paper

Parameter		Value	Units
Diameter of the level line	(d_l)	1.009×10^{-3}	m
Length of the line	(l)	4.8	m
Density of the line	(ρ_l)	1.158×10^3	kg m ⁻³
Density of air	(ρ_a)	1.29	kg m ⁻³
Normal drag coefficient of the fly line	(C_n)	1	
Tangential drag coefficient of the fly line	(C_t)	0.015	
Mass of the fly	(m_f)	0.000075	kg
Drag coefficient of the fly	(C_f)	1	
Radius of the fly	(r_f)	0.0075	m
Initial velocity	(v_0)	15	m s ⁻¹

Case #1: $\frac{D_{max}}{2} \leq R$

For a cast that begins with a loop of radius R larger than $D_{max}/2$, the steps above lead to the conclusion that the fly decelerates monotonically

$$\left(\frac{dv}{dx} < 0\right)$$

as the cast evolves (as x increases, or equivalently as $l(t)$ decreases). Thus, the energy dissipated by drag fully overcomes the tendency of the fly to accelerate in the absence of drag for these ‘large’ loops. Refer to Figure 4a which illustrates how the fly velocity decreases as the cast evolves.

Case #2: $\frac{D_{min}}{2} \leq R \leq \frac{D_{max}}{2}$

For a loop with radius R between $D_{min}/2$ and $D_{max}/2$, the behaviour is no longer monotonic. The fly first decelerates as the length of the traveling line decreases and then accelerates when the traveling line becomes shorter than

$$l_c = \frac{1}{2\lambda}(1 - 2\lambda\mu).$$

The final velocity of the fly can either be larger or smaller than the initial velocity of the traveling line. The intermediate case, when the initial and the final velocity are equal, is determined by the root of the equation

$$\left[\frac{1}{2} + \lambda(\beta - \mu)\right] \ln\left(\frac{l_0 + \beta}{2}\right) = \lambda l_0 \tag{19}$$

Equation (19) can be solved for a critical loop diameter D_c using the definitions of β , l , and μ given by equations (9)–(11). For loop diameters smaller than the critical loop diameter, the final fly velocity will be larger than the initial traveling line velocity. For loop diameters larger than the critical loop diameter, the final fly velocity will be smaller than the initial traveling line velocity. Example of these behaviors are illustrated in Figures 4 (b), (c), (d).

Case #3: $R \leq \frac{D_{min}}{2}$

For a cast that begins with a loop radius smaller than $D_{min}/2$, the steps above lead to the conclusion that the fly accelerates monotonically

$$\left(\frac{dv}{dx} > 0\right)$$

as the cast evolves. Thus, the tendency of the fly to accelerate in the absence of drag overcomes the energy lost by drag for these ‘small’ loops. Refer to Figure 4(e).

Table 1 lists the casting parameters used to obtain the results shown in Figure 4. The reader should note that the cast is rather short and that the tangential drag coefficient is set artificially low ($C_t = 0.015$) in order to achieve Case #3. Even under these conditions, $D_{min} = 8$ cm and forming such a ‘tight’ loop would be very challenging. The casting parameters for a longer cast or one with a reasonable tangential drag coefficient would likely lead to $D_{min} < 0$ rendering Case #3 simply unachievable. Thus, we suggest that under normal casting conditions, the goal of a good caster is to form a loop corresponding to Case #2 and preferably with a radius

$$\frac{D_{min}}{2} < R < \frac{D_c}{2}$$

in order to yield a net increase in fly velocity. Any loop radius larger than $D_c/2$ would necessarily lead to a net decrease in fly velocity.

Tapered fly line

Tapered lines are designed to weight the line for proper casting, and to enhance loop propagation and loop turnover. Tapered lines will be modelled in this section using a linearly varying line diameter over a portion of the line, as is achieved in practice. Figure 5 is a schematic of a typical linear taper that makes a smooth transition between the smaller diameter ‘tip’ section (diameter d_t) to the larger diameter ‘belly’ section (diameter d_b). The length of the tip section and the (front) taper section are l_t and l_{ft} , respectively. The method to obtain the fly velocity as a function of the length of the traveling line $l(t)$ is very similar to that used in Section 2, and only the important results will be given in this Section. A detailed derivation can be found in Gatti (2002).

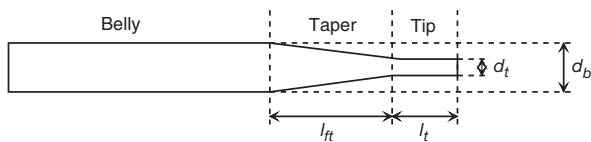


Figure 5 Schematic of a tapered line.

The work energy balance for a tapered line is

$$\frac{1}{2}m_{ti}(t)v^2(t) + \frac{1}{2}m_f v^2(t) + T_f(t) = T_0 - \int_0^t \delta \dot{W}_{ti}(u) du - \int_0^t \delta \dot{W}_f(u) du \quad (20)$$

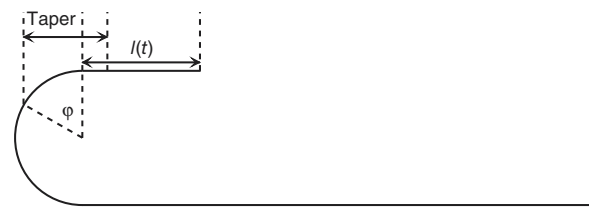
The integration of equation (20) recognizes three cases, depending on the position of the taper as illustrated in Figure 6. In particular, the integration progresses from the case where the taper is wholly within the traveling line, then partially within the traveling line and partially within the loop, and finally, wholly within the loop. The terms in equation (20) are detailed in Appendix C, and using these results, equation (20) can be rewritten as:

$$\frac{1}{2}M_i(l(t))v^2(t) = T_0 - \int_0^t \Gamma_i(l(u))v^3(u) du, \quad i \in \{1, 2, 3\} \quad (21)$$

Case # 1: $l_t + l_{ft} \leq l(t)$



Case # 2: $l_t \leq l(t) \leq l_t + l_{ft}$



Case # 3: $l(t) \leq l_t$



Figure 6 Three generic positions of the taper. (a) Taper wholly within traveling line, (b) taper partly within traveling line, (c) taper wholly within loop.

where

$$M_i(l(t)) = m_{ti}(t) + \frac{2T_{li}(t)}{v^2(t)} + m_f = \alpha_i(l(t)) + \beta_i \quad (22)$$

$$\Gamma_i(l(t)) = \frac{\delta \dot{W}_{ti}}{v^3(t)} + \frac{\delta \dot{W}_{li}}{v^3(t)} + \frac{\delta \dot{W}_{fi}}{v^3(t)} = \frac{\lambda_i \alpha_i}{2}(l(t) + \mu_i) \quad (23)$$

and $\alpha_i, \beta_i, \lambda_i$ and μ_i are given in Appendix C.

The fly velocity is then given by

$$v(l(t)) = v_0 \exp(\lambda_1(l(t) - l_0)) \left(\frac{l_0 - \beta_1}{l(t) + \beta_1} \right)^{1/2 + \lambda_1(\beta_1 - \mu_1)} \quad \text{for } l_t + l_{ft} \leq l(t) \quad (24)$$

$$v(l(t)) = v(l_t + l_{ft}) \exp\left(\int_{l_t + l_{ft}}^{l(t)} \frac{\Gamma_2(u)}{M_2(u)} du\right) \sqrt{\left(\frac{l_t + l_{ft} + \beta_2}{l(t) + \beta_2}\right)} \quad \text{for } l_t \leq l(t) \leq l_{ft} + l_t \quad (25)$$

$$v(l(t)) = v(l_t) \exp\left(\int_{l_t}^{l(t)} \frac{\Gamma_3(u)}{M_3(u)} du\right) \sqrt{\left(\frac{l_t + \beta_3}{l(t) + \beta_3}\right)} \quad \text{for } l(t) \leq l_t \quad (26)$$

and solution can be obtained by simple quadrature. Example results will be presented in the following Section.

Comparison with the numerical model

The analytical approximations presented above will now be compared with the numerical solutions obtained using the more general model presented in Gatti-Bono & Perkins (2002) and Gatti (2002). The line considered in this comparison is a double-tapered 5 weight floating line (DT-5-F) having the taper properties given in Table 2. The parameters used for the numerical simulation are summarized in Table 3 in reference to the discussion in Gatti-Bono & Perkins (2002).

Figure 7 illustrates the computed horizontal component of the fly velocity as a function of the dis-

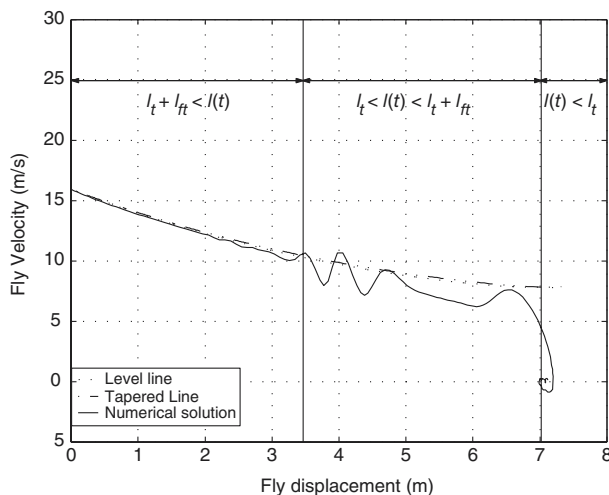


Figure 7 Comparison of numerical simulation (—) and approximate analytical solutions for a level line (...) and a tapered line (-.-.).

Table 2 Taper table for line DT-5-F

Section name	Length of the section (in m)	Diameter of the section (in m)
Tip	0.152	0.889×10^{-3}
Front taper	1.78	—
Belly	23.88	1.041×10^{-3}
Front taper	1.78	—
Tip	0.152	0.889×10^{-3}

Table 3 Data for the numerical model of fly casting; refer to Gatti-Bono & Perkins (2002)

Parameter	Symbol	Value	Units
Young's modulus	E	10^{10}	N m^{-2}
Length of the line	l	5	m
Density of the line	ρ_l	1.158×10^3	kg m^{-3}
Density of air	ρ_a	1.29	kg m^{-3}
Normal drag coefficient of the fly line	C_n	1	
Tangential drag coefficient of the fly line	C_t	0.075	
Coarse time step	Δt_1	0.0075	s
Fine time step	Δt_2	0.0002	s
Spatial step	Δs	0.0033	m
Prescribed error	Δe	0.05	
Mass of the fly	m_f	0.000075	kg
Drag coefficient of the fly	C_f	1	
Radius of the fly	r_f	0.0075	m
Diameter of equivalent level line	d_l	1.009×10^{-3}	m

placement of the fly. In this example, $R = 0.3625$ m is the chosen loop radius. This value of R would correspond to Case #2 in Section 2.2 if the fly line were *level* instead of *tapered*. The diameter of the equivalent line is taken to be the (spatial) average of the same length of tapered line and thus the level and tapered lines have equivalent mass and length. The parameters (D_{min} , D_{max} , D_c , l_c) discussed in Section 2.2 for this equivalent level line are given in Table 4. Note that for this cast:

$$\frac{D_c}{2} < R < \frac{D_{max}}{2}$$

and a net decrease in fly velocity is expected. The dotted curve is the analytical solution for the equivalent level line, the dash-dotted line is the analytical solution for the tapered line, and the solid line is the numerical simulation. First, it is interesting to note that the analytical solutions for a tapered line and for a level line are very similar. In the study by Spolek (1986), the graphs showed a significant difference

Table 4 Parameters that characterize a level line equivalent to the tapered line presented in this paper

Parameter	Value	Units
D_{min}	-3.425	m
D_{max}	0.909	m
D_c	-0.038	m
l_c	0.1559	m

between the behaviours of a level and of a tapered line, especially at the end of the cast. The discrepancy between the results found by Spolek (1986) and the results here can be ascribed to the different models for the tapered line, as well as the fact that the kinetic energy of the loop is not accounted for by Spolek (1986). The numerical simulation compares very well to the analytical solutions in the first region where the taper is wholly within the traveling line ($l_f + l_t \leq l(t)$). However, as soon as part of the taper enters the loop ($l_t < l(t) < l_t + l_f$), the numerical simulation and the analytical solutions diverge. In particular, the numerical solution shows that the fly velocity generally decreases but not monotonically. Moreover, the final horizontal velocity decreases rapidly during loop turnover and this is not captured in the approximate solutions. The major reason for this divergence is that the analytical model makes considerably more simplifying assumptions that are not made in the numerical solution. These include assuming a perfectly circular loop, a constant loop diameter (that is also prescribed), a prescribed (straight) path of the traveling line, and a stationary (lower) part of the fly line. Overall, these assumptions prevent the analytical solutions from accurately describing the physics of the loop turnover as the taper enters the loop ($l_t < l(t) < l_t + l_f$) and where the taper lies wholly within the loop ($l(t) < l_t$).

Summary and conclusion

This paper presents an analytical approach to modelling loop propagation for a fly cast and a critical comparison with a numerical solution. For the analytical solution, the geometry of the loop and all the other portions of the fly line are prescribed in advance. A work-energy balance relates the velocity of the fly to the length of traveling line. A critical loop diameter,

that depends on the density and geometry of the fly line and the fly line air drag is identified. This loop diameter determines whether the final velocity of the fly will be greater or lesser than its initial velocity. The numerical solution is critically compared to the analytical solutions. When the taper is in the traveling line (the loop propagation phase), the agreement between the two solutions is very good (within 10%). However, as soon as the taper enters the loop, the two solutions diverge because of the many simplifying assumptions made in the analytical model. In particular, the analytical model should not be used to study final loop turnover.

Appendix A: level line

$$T_l(t) = \frac{1}{2} \frac{\rho_l \pi^2 d_l^2 R v^2(t)}{8} \tag{27}$$

Where R is the loop radius defined in Figure 2.

$$\delta \dot{W}_t(t) = \frac{1}{2} \rho_a C_t d_t \pi l(t) v^3(t) \tag{28}$$

where ρ_a is the density of air and C_t the tangential drag coefficient of the fly line.

Following Lingard [5],

$$\delta \dot{W}_l(t) = \rho_a d_l R \left(\frac{5\pi^2}{32} C_t + \frac{1}{12} C_n \right) v^3(t) \tag{29}$$

Where C_n is the normal drag coefficient of the fly line.

$$\delta \dot{W}_f(t) = \frac{1}{2} \rho_a C_f \pi r_f^2 v^3(t) \tag{30}$$

where r_f is the radius of the fly and C_f the drag coefficient of the fly.

Appendix B: on the integration of (13)

Replacing $M(l(t))$, $\Gamma(l(t))$, and $M'(l(t))$ by their expressions as functions of α , β , λ and μ , equation (13) becomes

$$\alpha \left(l(t) + \beta \right) \ddot{l}t = \left(\alpha \lambda (l(t) + \mu) - \frac{1}{2} \alpha \right) \dot{l}^2(t) \tag{31}$$

The change of variables $\dot{l}(t) = z(l)$ yields

$$\ddot{l}(t) = \frac{dz}{dt} = \frac{dz}{dl} \frac{dl}{dt} = z \frac{dz}{dl} \tag{32}$$

and equation (31) can be rewritten

$$(l(t) + \beta) z \frac{dz}{dl} = \left(\lambda(l(t) + \mu) - \frac{1}{2} \right) z^2 \quad (33)$$

Since the fly is propagating, $\dot{l}(t)$ and therefore z are not equal to zero, and we can divide equation (33) by z

$$(l(t) + \beta) \frac{dz}{dl} = \left(\lambda(l(t) + \mu) - \left(\frac{1}{2} + \lambda(\beta - \mu) \right) \right) z \quad (34)$$

Equation (34) is solved by separating variables and then integrating between l_0 and $l(t)$ to give

$$\ln \frac{z(l)}{z(l_0)} = \lambda(l(t) - l_0) - \left(\frac{1}{2} + \lambda(\beta - \mu) \right) (l(t) - l_0) \quad (35)$$

Equation (14) follows

$$v(l(t)) = v_0 e^{(\lambda(l(t) - l_0) - (\frac{1}{2} + \lambda(\beta - \mu))(l(t) - l_0))} \quad (36)$$

Appendix C: tapered line

Let d_b , d_t , l_t and l_{ft} be the design parameters of the tapered fly line shown in Figure 5. Then,

$$\begin{aligned} M_1(l(t)) &= \rho_l \frac{\pi}{4} \left(d_t^2 l_t + d_b^2 (l(t) - l_{ft} - l_t) \right) \\ &+ \frac{l_{ft}}{3} (d_b^2 + d_t^2 + d_t d_b) + \frac{\rho_l \pi^2 d_b^2 R}{8} + m_f \\ &= \alpha_1(l(t) + \beta_1) \end{aligned} \quad (37)$$

$$\begin{aligned} \Gamma_1(l(t)) &= \frac{1}{2} \rho_a C_t \pi \left(d_b l(t) - \left(\frac{l_{ft}}{2} + l_t \right) (d_b - d_t) \right) \\ &+ \rho_a d_b R \left(\frac{5\pi^2}{32} C_t + \frac{1}{12} C_n \right) + \frac{1}{2} \rho_a C_f \pi r_f^2 \\ &= \frac{\lambda_1 \alpha_1}{2} (l(t) + \mu_1) \end{aligned} \quad (38)$$

$$m_{d_2}(t) = \rho_l \frac{\pi}{4} \left(d_t^2 l(t) + d_t \frac{d_b - d_t}{l_{ft}} (l(t) - l_t) \right)$$

$$+ \left(\frac{d_b - d_t}{l_{ft}} \right)^2 \frac{(l(t) - l_t)^3}{3} \quad (39)$$

Let φ be the angle depicted in Figure 6(b). Then

$$\varphi = \frac{l_{ft} + l_t - l(t)}{R} \quad (40)$$

$$\begin{aligned} T_{l_2}(t) &= \frac{\rho_l R \pi v^2(t)}{48 l_{ft}^2} (R^2 (d_b - d_t)^2 (6\varphi + \varphi^3 - 6\sin(\varphi)) \\ &- 3R l_{ft} d_b (d_b - d_t) (2 + \varphi^2 - 2\cos(\varphi)) + 3\pi l_{ft}^2 d_b^2) \end{aligned} \quad (41)$$

$$\delta \dot{W}_{t_2} = \frac{1}{2} \rho_a C_t \pi \left(d_t l(t) + \left(\frac{d_b - d_t}{l_{ft}} \right) \left(\frac{l(t) - l_t}{2} \right) \right) v^3(t) \quad (42)$$

$$\begin{aligned} \delta \dot{W}_{l_2} &= \frac{\rho_a R C_n}{576 l_{ft}} \left(48 d_b l_{ft} - R(d_b - d_t) \right) \\ &\left(24\varphi - 27\sin(\varphi) + \sin(3\varphi) \right) v^3(t) \end{aligned} \quad (43)$$

$$\begin{aligned} &+ \frac{\rho_a \pi R C_t}{1152 l_{ft}} \left(180\pi d_b l_{ft} - R(d_b - d_t) (299 + 90\varphi^2 \right. \\ &\left. - 270\cos(\varphi) - 27\cos(2\varphi) + 2\cos(3\varphi)) \right) v^3(t) \end{aligned} \quad (44)$$

Let φ and ψ be the angles depicted in Figure 6(c). Then

$$\psi = \frac{l_t - l(t)}{R} \quad (45)$$

$$\varphi = \psi + \frac{l_{ft}}{R} \quad (46)$$

$$\begin{aligned} Tl_3(t) &= \frac{\rho_l \pi v^2(t)}{48 l_{ft}^2} \left(6R^3 (d_b - d_t)^2 (\sin(\psi) - \sin(\varphi)) \right. \\ &- 6R^2 l_{ft} d_t (d_b - d_t) \cos(\psi) + 6R^2 l_{ft} d_b (d_b - d_t) \cos(\varphi) \\ &- l_{ft}^3 (d_b - d_t) (d_t + 2d_b) - 3R \alpha l_{ft}^2 (d_b^2 - d_t^2) \\ &\left. + 3R \pi l_{ft}^2 d_b^2 \right) \end{aligned} \quad (47)$$

$$\delta \dot{W}_{t_3} = \frac{1}{2} \rho_a C_t \pi d_t l(t) v^3(t) \quad (48)$$

$$\begin{aligned} \delta \dot{W}_{t_3} = & \frac{\rho_a R C_n}{576 l_{ft}} \left(24 l_{ft} (d_b + d_t) + R(d_b - d_t) \right. \\ & \left. \left(27(\sin(\varphi) - \sin(\psi)) + \sin(3\psi) - \sin(\varphi) \right) \right) v^3 t \\ & + \frac{\rho_a \pi R C_t}{1152 l_{ft}} \left(180 R d_b \pi l_{ft} - 90 l_{ft}^2 (d_b - d_t) + R^2 (d_b - d_t) \right. \\ & \left. \left(270(\cos(\varphi) - \cos(\psi)) + 27(\cos(2\varphi) - \cos(2\psi)) \right) \right. \\ & \left. + 2(\cos(3\varphi) - \cos(3\psi)) \right) - 180 R l_{ft} \alpha (d_b - d_t) \left. \right) v^3(t) \quad (49) \end{aligned}$$

The power dissipated by drag acting on the fly remains as given by equation (30).

Acknowledgment

The authors wish to acknowledge the supplies and the many insightful technical discussions offered by Mr. Bruce Richards of Scientific Anglers and the Rackham Predoctoral Fellowship offered by the Horace H. Rackham School of Graduate Studies at the University of Michigan.

References

- Gatti, C.S.C. (2002) *Numerical Simulations of Large Deformation Cable Dynamics*, PhD Dissertation, University of Michigan.
- Gatti, C.S. & Perkins, N.C. (2001) 'Numerical analysis of flycasting mechanics', *ASME Bioengineering Conference*, BED-Vol. 50, pp. 277–278, Snowbird, UT.
- Gatti-Bono, C. & Perkins, N.C. (2002) 'Physical and Numerical Modeling of the Dynamic Behavior of a Fly Line', *Journal of Sound and Vibration*, **255**(3), pp. 555–577.
- Hendry, M.A. & Hubbard, M. (2000) 'Dynamic finite element simulation of fly casting and its potential use in fly rod design', *The Engineering of Sport: Research, Development and Innovation*, Blackwell Science, Oxford, pp. 407–414.
- Lingard, S. (1988) 'Note on the aerodynamics of a fly line', *American Journal of Physics*, **56**(8), pp. 756–757.
- Robson, J.M. (1990) 'The physics of flycasting', *American Journal of Physics*, **58**(3), pp. 234–240.
- Spolek, G.A. (1986) 'The mechanics of flycasting: The fly line', *American Journal of Physics*, **54**(9), pp. 832–835.